PHYSICAL REVIEW B VOLUME 25, NUMBER 6 15 MARCH 1982

Electronic properties of graphite: A unified theoretical study

R. C. Tatar and S. Rabii
Moore School of Electrical Engineering and Laboratory for Research on the Structure of Matter, University of Pennsylvania, Philadelphia, Pennsylvania 19104
(Received 31 August 1981)

We have calculated the electronic structure of three-dimensional graphite using the modified first-principles Korringa-Kohn-Rostoker technique developed for and applied to the intercalation compound LiC_6. Whereas previous calculations of the electronic band structure of graphite provide explanations either for moderate- to high-energy excitations or for low-energy and Fermi-surface properties, we find excellent agreement between our results and experiments in both regimes. Our analysis of the band structure is based on a comparison with experiments of predicted optical transitions, values for the Slonczewski-Weiss-McClure parameters which we obtain from a fit to our bands, and Fermi-surface properties. We also present a density of states for our band structure and several constant-energy surfaces. Our discussion includes a comparison with other theoretical work.

I. INTRODUCTION

Crystalline carbon in the form of graphite is one of the most extensively studied materials both experimentally and theoretically. Because of its layered structure with a relatively large separation between layers, graphite is often modeled as a two-dimensional solid. This is very convenient for calculations and has been studied with tight-binding (TB),[1-6] linear combination of atomic orbitals (LCAO),[7] orthogonalized-plane-wave—tight-binding (OPW-TB),[8,9] generalized OPW,[10,11] self-consistent extended Hückel,[12] exact exchange Hartree-Fock,[13] and other techniques.[14] The single-layer model necessarily ignores interlayer interactions which introduce band splittings of roughly 1 eV and introduce important structure near the Fermi level. Thus low-energy optical properties, transport, and other fine-structure-dependent electronic properties are not adequately covered by these calculations.

The previous calculations of the three-dimensional graphite band structure can be divided into two categories. First there are the band structures which are fitted in detail to experimental results over a small energy range. These provide accurate information about the Fermi surface and are useful for correlating transport related measurements[1,15] and explaining optical structure at moderate energies.[16] This type of calculation is often used to supplement the single-layer calculations.[1,5,7,9,11] Zunger[12] has provided a comparison of many of the above calculations. In the second category of three-dimensional calculations, a much wider energy range and a much larger portion of the Brillouin zone is covered. The methods used range from TB,[17] LCAO,[18] pseudopotentials,[19,20] to cellular.[21] While higher-energy optical properties are potentially better predicted, in general, these calculations are not sufficiently accurate to provide an adequate representation of the Fermi surface.

The above classification also applies to experimental techniques. The Fermi surface and Fermi-surface parameters have been studied by de Haas—van Alphen effect[15,22-25] magnetoreflection,[26] cyclotron resonance,[27-29] magnetic susceptibility,[22] and various other techniques,[30-32] while higher-energy properties have been measured using photoemission,[33-35] secondary electron emission,[36] electron spectroscopy for chemical analysis,[37-39] soft x rays,[40] electron-energy loss,[41] reflectivity,[42-44] thermoreflectivity,[45] optical absorption.[46] The review articles by Spain[30,31] and McClure[32] provide a detailed study of the low-energy properties.

In the present study we produce an accurate *ab initio* energy-band structure for three-dimensional graphite that combines the features of both types of calculation. In other words, it not only provides the energy bands over a large energy range, it also leads to a very reasonable model for Fermi-surface properties of this material.

Due to the structural similarity of graphite and the graphite-intercalation compounds, we chose for

this study the modified Korringa-Kohn-Rostoker (KKR) approach of Holzwarth *et al.* that was developed and successfully applied to LiC_6,[47] and subsequently to KC_8.[48] Since graphite has been extensively studied in the past, a detailed evaluation of our results, and thus the formalism, is possible and this has important implications for our studies of the graphite-intercalation compounds.

II. GRAPHITE STRUCTURE AND POTENTIAL

The structure of graphite chosen for this study is the *AB* or Bernal structure[49] (Fig. 1). It consists of planes of carbon atoms, each forming a hexagonal net, stacked in a manner such that half of the carbons (*A* atoms) are located directly above each other in adjacent planes, while the other half (*B* atoms) are located above the center of the hexagon in the adjacent plane.[50] There are four atoms per unit cell, two of the inequivalent *A* and *B* carbons (Fig. 2).

The space group G_s of graphite is $P6_3/mmc$.[51] The corresponding point (factor) group, $P = G_s/T$, has 24 elements and is isomorphic to D_{6h}. T denotes the lattice (translation) group. This structure contains two inequivalent inversion centers, one located halfway between adjacent layers on a *c*-axis line through *A* carbons, while the other is obtained from the former by half a primitive translation perpendicular to the *c* axis.

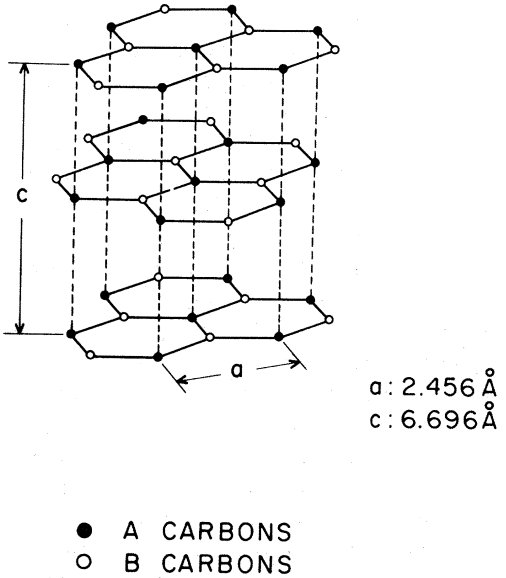

FIG. 1. Graphite structure. Lattice constants from Ref. 50.

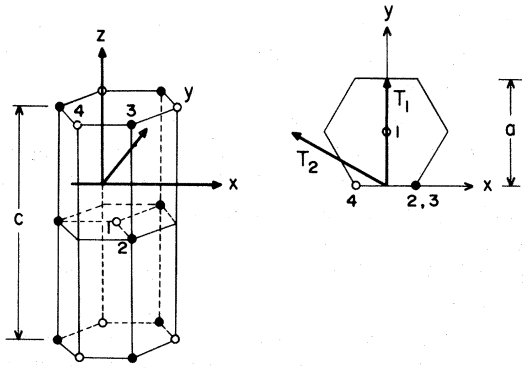

FIG. 2. Graphite unit cell and coordinate system for present work.

The local symmetry about the atoms in the unit cell enters certain aspects of the calculation such as the computation of wave functions near a site using a symmetry eigenfunction expansion. While the potentials for the *A* and *B* atoms are not identical, the local symmetry for both is described by the group D_{3h}.

The Brillouin zone of the reciprocal lattice is shown in Fig. 3 with the high-symmetry point and directions labeled. The groups of k vectors at the top and bottom surfaces of the zone have only even-dimensional representations.[52] Likewise, for points in the interior of the zone (except at Γ) the representations are all one dimensional.

The crystal potential was constructed by linear superposition of carbon self-consistent field, Hartree-Fock-Slater charge densities.[53] Since the band-structure calculation was not self-consistent, it was important to obtain as realistic a crystal potential as possible. Thus in order to reflect the in-plane bonding of carbon atoms, the atomic charge

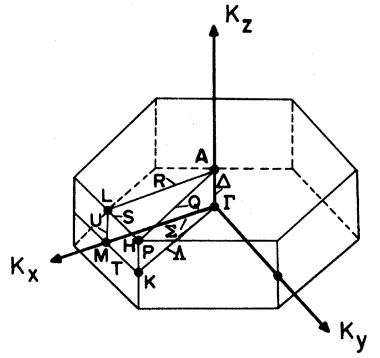

BRILLOUIN ZONE

FIG. 3. Brillouin zone of graphite.

density of carbon was calculated using a $2s^2 2p^2$ configuration. Previous experience, however, indicated that the crystal potential would be only slightly affected by changes in the neutral atomic configuration and the exchange-correlation approximation. The exchange-correlation potentials both in atomic and crystal calculations are obtained using the local $X\alpha$ statistical prescription of Slater[54] with the value of 0.759 for α as obtained by Schwartz.[55]

The results of the above procedure are displayed in Fig. 4 where the potential is shown along three directions. While the potential is nearly spherically symmetric close to the atomic sites, its angular variation is greater than 1 Ry at a distance of one-half the nearest-neighbor spacing (muffin-tin radius). Such a large potential anisotropy is typical also of graphite-intercalation compounds where we have applied our present approach to calculate their electronic properties.[47,48] How well our band-structure formalism performs under such conditions is one of the objectives of this work.

III. BAND-STRUCTURE CALCULATION

The technique used for the calculation of energy bands was a modified version of Painter's discrete variational KKR method procedure.[56–58] This method was developed by Holzwarth *et al.* (HRG) and applied to LiC_6 (Ref. 47) and later to KC_8.[48] In the first step of the HRG approach a modified KKR calculation is performed on a muffin-tin form of the crystal potential, V_{MT}. This is followed in the second step by diagonalizing the non-muffin-tin Hamiltonian in the muffin-tin basis. The reader is referred to Refs. 47 and 48 for the details of the formalism.

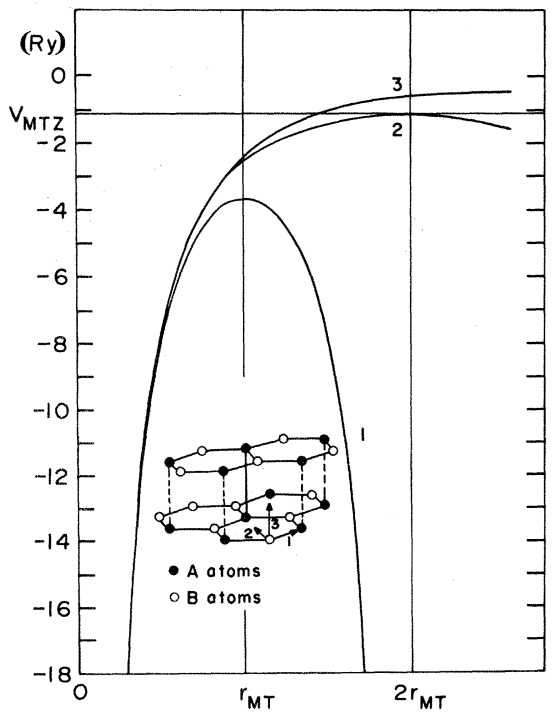

FIG. 4. Crystal potential.

In the interstitial region the constant potential value or muffin-tin zero (V_{MTZ}) is taken to be the volume-averaged potential of that region and in the present work is 1.119 Ry below the atomic (carbon) zero level. The band structure for the full crystal potential, i.e., our final band structure, does not depend on V_{MTZ}. The radius of the MT spheres, r_{MT}, is chosen so that the atomic spheres touch but do not overlap. In graphite $r_{MT}=1.34$ a.u. and the interstitial region occupies 83% of the unit cell. This is a much larger fraction than for the intercalation compounds LiC_6 and KC_8 where the corresponding numbers are 54% and 43%. Because the interstitial region is so large, with a corresponding large potential fluctuation, it is clear that a muffin-tin calculation by itself is inappropriate for graphite energy bands.

The reaction operator $\mathcal{K}_{ij}^{\sigma\,-1}$ [Eq. (1), Ref. 48] at the σth sphere gives the relative scattering of the ith (incident wave) component of the jth eigenfunction. In general the reaction operator $\mathcal{K}_{lm,l'm'}^{\sigma\,-1}$ is a complicated function of energy which is evaluated on a coarse energy grid in the angular-momentum representation. For graphite, however, it was found that the reaction matrix components are very smooth functions of energy over the range considered. This is in contrast to previous calculations[47,48] where many singularities were present. This smoothness permitted rapid and very accurate numerical interpolation and extrapolation.

The results of the first step of the calculation (modified KKR procedure) are displayed in Fig. 5. Many symmetry-dependent features are visible such as the degeneracies of the bands at K and H and the nearly free-electron-like shapes of the lower σ and π bands. The muffin-tin potential, however, exaggerates many level separations and causes level crossings that do not occur in the final bands. From the position of V_{MTZ} it is expected that the dominant distortion is a larger band dispersion along the $\vec{k}_z$ directions but the band shapes perpendicular to $\vec{k}_z$ will be very similar in the non-muffin-tin bands. This is because the

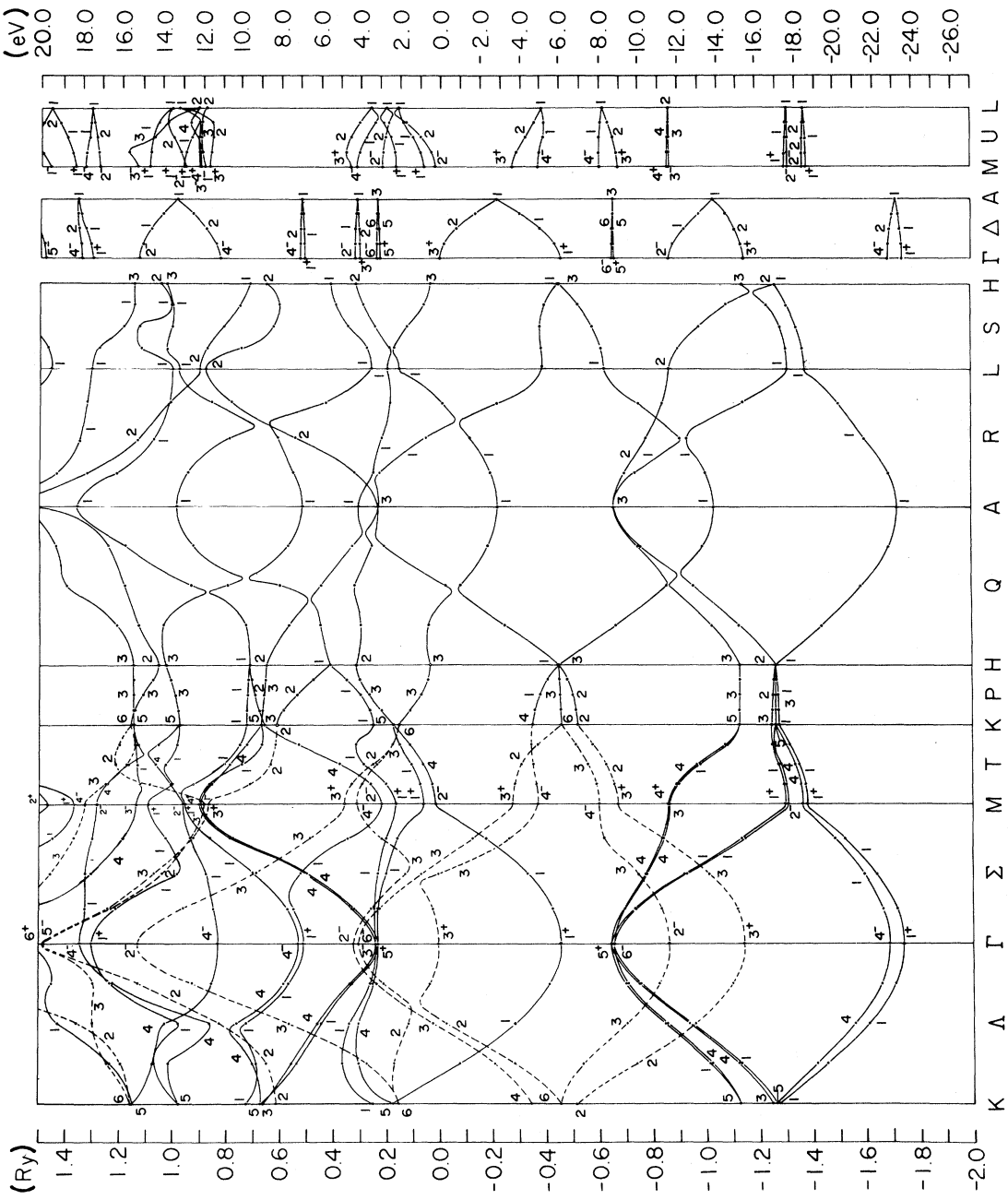

FIG. 5. Muffin-tin band structure (KKR).

muffin-tin zero lies between the potential extrema of the directions parallel and perpendicular to the layers. Thus, on the average the c-axis muffin-tin potential is more attractive than the exact potential and conversely the in-plane muffin-tin potential is more repulsive. This means that interlayer interactions between the p_z orbitals that are responsible for the splittings are overestimated by the muffin-tin potential, increasing the $\vec{k}_z$ dispersion.

In practice the secular equation [Eq. (1), Ref. 48] includes all l,m for which scattering is large. Previous work[47] showed than an s-p expansion is quite accurate and in almost all situations an expansion including d waves is extremely good. For this study components up to $l=2$ have been included. This is sufficient to obtain bands of all symmetries since all irreducible representations of groups of k have explicit representations in terms of atomic centered spherical harmonics of $l=0$, 1, or 2. In order to estimate the effect of the d-wave components, the reaction matrix and KKR eigenenergies were recomputed at Γ and M excluding $l=2$ terms. As anticipated there was no change in the π levels. Except for the Γ_5^+,Γ_6^- levels which moved by about 1.5 eV, most of the σ levels differed from the s-p-d KKR levels by less than 0.9 eV. However, we expect these shifts to be much reduced in the final non-muffin-tin bands since, in general, the d-wave scattering is exaggerated by the muffin-tin potential due to the orientation of these orbitals and their larger spatial extension into the interstitial region.

The results of the HRG procedure for the potential and structure described in Sec. II are shown in Fig. 6. The symmetry labels are those of Slater.[59]

The bands were obtained at 33 wave vectors along the edges of an irreducible sector of the Brillouin zone including all the high-symmetry points and direction. The bands on the hexagonal face of the zone (H-A-L-H) are all doubly degenerate and look much like the bands from single-layer calculations.

Most of the KKR levels were found within 0.01 mRy tolerance so the accuracy of the non-muffin-tin bands was limited by the accuracy of the potential matrix elements Δ_{NM} [Eq. (3), Ref. 48]. The position of the upper non-muffin-tin bands, i.e., those with energies about 1.3 Ry, however, should be considered as very approximate due to the necessity of truncating the non-muffin-tin secular matrix [Eq. (2), Ref. 48]. The KKR searches were taken up to at least 2 Ry above V_{MTZ} at each of the 33 wave vectors.

IV. DENSITY OF STATES AND FERMI-SURFACE PROPERTIES

A. Interpolation models

In order to analyze the implications of a given band-structure calculation for experimentally measurable phenomena, it is often necessary to perform integrations over the Brillouin zone that require knowledge of the energy bands at each k point.[60] It is extremely expensive to evaluate the eigenspectrum for a large number of wave vectors using the method outlined in Sec. III, so a physically sensible and accurate intepolation scheme is highly desirable.

In graphite it is known from experimental and theoretical studies that the bands near the Fermi level play a dominant role in transport and low-energy optical properties. A parametrized model for these bands would provide a useful interpolation scheme.

There are two currently well-known models for graphite: (1) the Slonzcewski-Weiss-McClure (SWMc) model[15] for Fermi-level bands near the H-K axis and (2) the full zone π-band Johnson-Dresselhaus (JD) model.[16] Both models are described below with additional details given in Appendices A and B.

The Slonzcewski-Weiss-McClure (SWMc) model originated about 25 years ago[5] as a tight-binding $k\cdot p$ analysis specifically for the Fermi-level bands of graphite, near the H-K axis of the Brillouin zone. This work was reexamined by McClure,[15] who demonstrated that seven parameters (SWMc parameters) adequately described the shape of the bands and the Fermi surface. This very useful analytical tool immediately became popular among experimentalists and many experimental results are still expressed in terms of these parameters.

A least-square fitting procedure with a modified gradient search[61] was used to determine the values of the SWMc parameters from the bands shown in Fig. 6. The energy levels at 6 $\vec{k}$ points including H, K, and a Λ point were used in the fit. Several types of weighting schemes were tried and all gave roughly the same results. The numbers are shown in Table I. The parameters of column a were computed with approximately equal percentage error and most accurately reflect the shapes and position of the *ab initio* bands. Column b parameters were found with equal absolute error and are not as good for parameters with small magnitude. There is a change of sign of the Δ parameter and γ_2

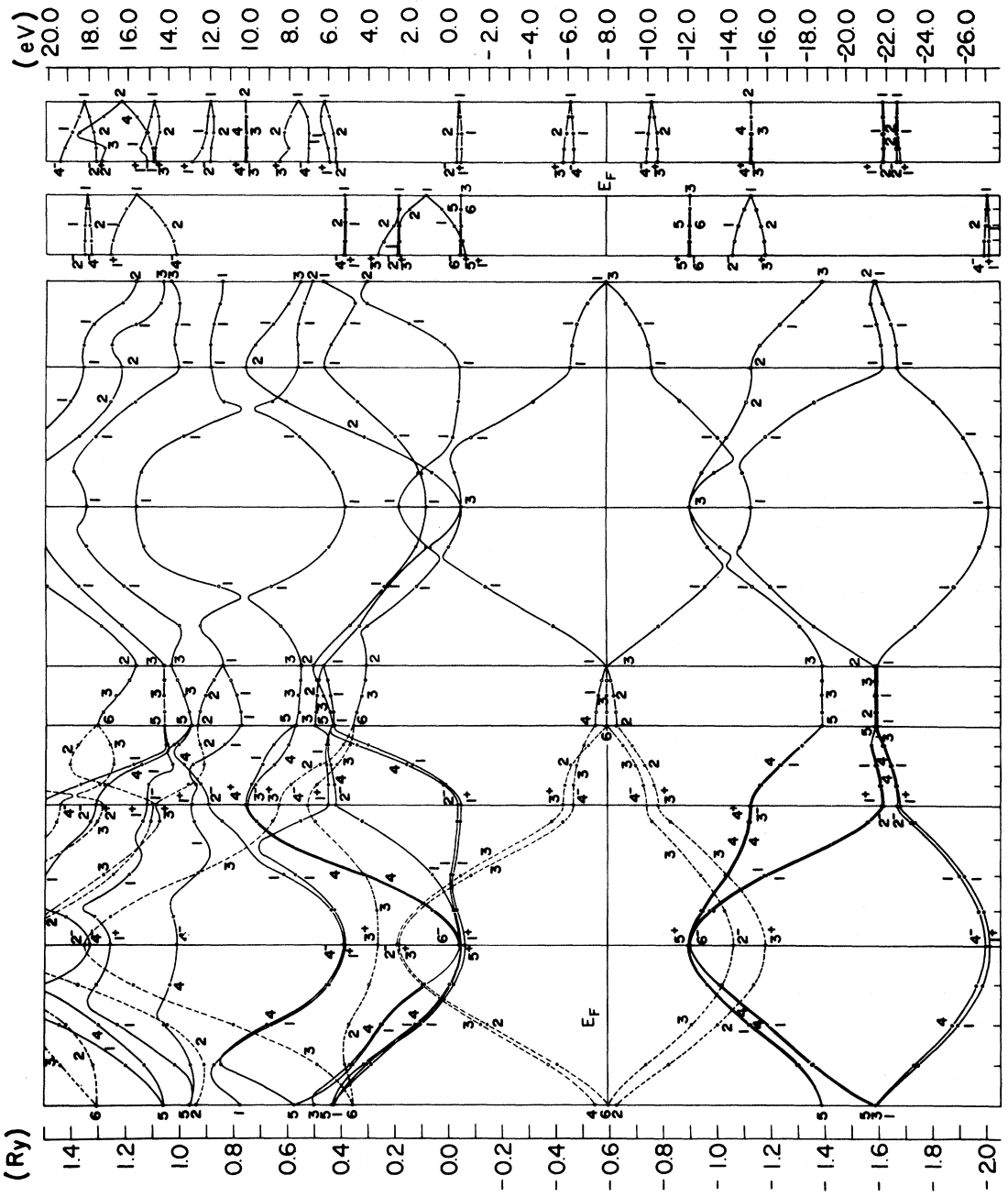

FIG. 6. Band structure of three-dimensional graphite (full crystal potential). π bands are dashed.

TABLE I. SWMc parameters for graphite (eV).

	a	b	c	d
γ_0	2.92	2.92	2.41	3.16
γ_1	0.27	0.27	0.27	0.39
γ_2	−0.022	−0.009	−0.022	−0.019
γ_3	0.14	0.15	0.14	0.28
γ_4	0.10	0.10	0.074	0.044
γ_5	0.0063	0.029	0.0065	0.038
Δ	−0.0079	−0.0085	0.0074	−0.008
E_F	−0.025			−0.024

[a]Weighted least-squares fit to *ab initio* bands (preferred); SWMc model.
[b]Equal weight least-squares fit; SWMc model.
[c]Estimated from full-zone fit to *ab initio* bands using Johnson-Dresselhaus model Hamiltonian.
[d]Experiments, Ref. 70.

grows at the expense of γ_5. Finally the column c parameters were estimated from the parameters of the full-zone JD model using the formulas as given in Appendix B (see Table VII).

The differences in the parameters reflect different emphasis of the bands. For example, the column c parameters arise from a fit that should be suitable for analysis of optical properties between 2−12 eV, while the a column parameters should accurately reflect transport properties. We feel the SWMc model is unable to consistently account for both transport and optical properties with the same parameters and there is some experimental evidence to suggest this. It is not clear, however, that simply adding higher-order terms will be useful.

Figure 7 demonstrates the accuracy of the SWMc fit along the *H-K* axis. The *H* and *K* point levels were fit exactly and the differences between the *ab initio* bands and SWMc arise from slightly different dispersion along *P*. In this sense we have an *ab initio* verification of SWMc. We expect an even greater difference off the *H-K* axis but can make no accurate comparison because the nearest *ab initio* off-axis $\vec{k}$ point is near the limit of validity of the SWMc model.

The JD model Hamiltonian[16] is based on a full-zone symmetrized Fourier (tight-binding) expansion of the π bands and was shown to be equivalent to the SWMc model along the *H-K* axis. In fact, in the original study where an analysis of optical properties was performed, this equivalence was used to determine the full-zone expansion parameters (JD parameters) from a set of experimentally determined SWMc parameters.

By performing a unitary transformation $H_M = SH_{\rm JD}S^{-1}$ on the JD Hamiltonian with

$$S = \begin{bmatrix} \frac{1}{\sqrt{2}} & \frac{-1}{\sqrt{2}} & 0 & 0 \\ \frac{-1}{\sqrt{2}} & \frac{1}{\sqrt{2}} & 0 & 0 \\ 0 & 0 & 1 & 0 \\ 0 & 0 & 0 & 1 \end{bmatrix},$$

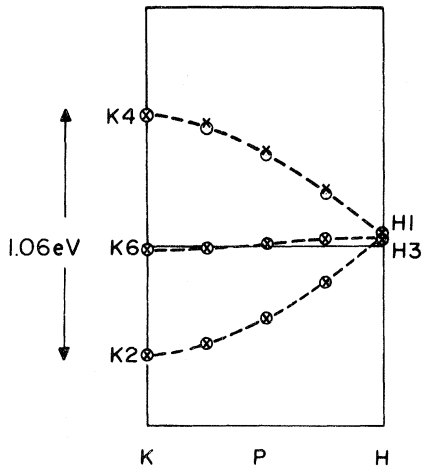

FIG. 7. Comparison of first-principles bands with SWMc fit, × SWMc fit, o *ab initio* bands. Most of the points overlap completely on scale shown.

one arrives at a form that can be compared with McClure's Hamiltonian and the SWMc parameters can be extracted from the JD parameters. Performing this algebra we find the relationships given in Appendix C.

It is well known that the eigenvalues of the SWMc Hamiltonian are invariant under simultaneous change of sign of γ_0 and γ_4. The JD Hamiltonian also has this property and is invariant under simultaneous change of sign of the "off-diagonal parameters": a_{AB}^{010}, a_{AB}^{020}, a_{AB}^{120}, a_{AB}^{011}. Such changes in sign might be brought about indirectly by coordinate system changes. Thus the sign of γ_0 and γ_4 are not given uniquely by this theory.

A least-squares fit (modified gradient search)[61] to the band structure along *K-H*, *K-M*, and towards Γ gave the parameters in Table II. Our parameters differ a great deal from those given by Johnson and Dresselhaus[16] and equivalent parameters given by Holzwarth[62] based on the two-dimensional band structure of Painter and Ellis. Part of this difference between our parameters and those from previous works is due to the difference in our energy scale zero (diagonal constants). Another factor contributing to this difference is that the previous fits were to bands near the rectangular faces of the Brillouin zone—unconstrained in the zone center—and the best fits to these bands caused an excessive bandwidth at Γ, between the top of the conduction band and the bottom of the valence band.

B. Density of states

The JD model has been used to give a satisfactory account of the infrared optical properties of graphite.[16] Recently Holzwarth[62] used an extension of the JD model for a layer analysis of intercalation compounds of graphite. It was because of these successes that the JD model was chosen as a full-zone interpolation of the *ab initio* bands of Sec. III. This fit was expected to provide a reasonably accurate density of states from the band structure because of the large number (11) of adjustable parameters.

The density of states was obtained from the histogram method, which uses the approximate expression:

$$g_{\Delta E}(E)=\frac{2}{(2\pi)^3}\times\sum_{\alpha}\frac{1}{\Delta E}\int_{E}^{E+\Delta E}\left[\int\delta(E_\alpha(\vec{k})-E)d\vec{k}\right]dE\ , \tag{1}$$

where the α sum is over the valence and conduction π bands.

Roughly 20 000 points in an irreducible sector of the Brillouin zone were used with a higher density of points concentrated in a wedge near the *H-K* axis than in the rest of the zone. This provided a

TABLE II. JD parameters (eV).

	Parameter	Used for Fig. 9 *H-K* fit	Full-zone fit
1	a_{AA}^{000}	−3.38	−3.29
2	a_{AA}^{100}	−1.43	−1.18
3	a_{BB}^{000}	−1.83	−1.79
4	a_{BB}^{100}	1.68	1.85
5	a_{AB}^{010}	−2.14	−2.20
6	a_{AB}^{020}	0.0450	0.0442
7	a_{AB}^{120}	0.364	0.362
8	$a_{AA'}^{001}$	0.181	0.143
9	$a_{BB'}^{011}$	0.272	0.279
10	$a_{AB'}^{011}$	0.148	0.157
11	a_{AA}^{002}	0.0022	0.0104
12	a_{BB}^{002}	−0.0072	0.0110

smooth curve near the valence-conduction junction where in addition the interval ΔE was decreased.

The π density of states calculated from (1) is shown in Fig. 8. The overall shape is as expected. The width of 19 eV is a bit larger than the width of the actual π bands because of the slight inaccuracy of the fit which was weighted to more accurately fit the bands along the *L-M-K-H* face of the zone. As a self-consistent check the area under the curve was computed and found to be exactly two electrons per carbon. The peaks correspond to the *M* point dispersion and would be singular in a single-layer calculation. The peak separation is 4.3 eV on average but varies between 3.8 and 4.7 and corresponds to the 4.6 eV critical transition observed experimentally. The density of states is in qualitative agreement with that of Painter and Ellis,[7] Samuelson and Batra,[17] and Zunger.[12]

Also included in Fig. 8 for comparison is the density of states obtained from a fit to SWMc. SWMc is expected to be more accurate in a region near the minimum of roughly 200 meV in width but can be seen to rapidly diverge from the more accurate overall calculation thereafter. Although a more extensive fit to the *ab initio* bands might reduce this discrepancy somewhat, this difference was expected from the nature of the SWMc model which is limited to a small region of reciprocal space.

The conventional approach for obtaining the Fermi energy is to integrate the density of states up to the required number of carriers. The JD model, however, is inaccurate in the region of the Fermi level and the SWMc model is very inaccurate near the π-band edges. For this reason we proceeded by requiring the number of electrons and holes to be equal, leading to a Fermi level of -0.025 eV. As a check we also integrated the JD density of states up to 1 electron and found a value of -0.09 eV. This is close but too low to give a realistic Fermi surface.

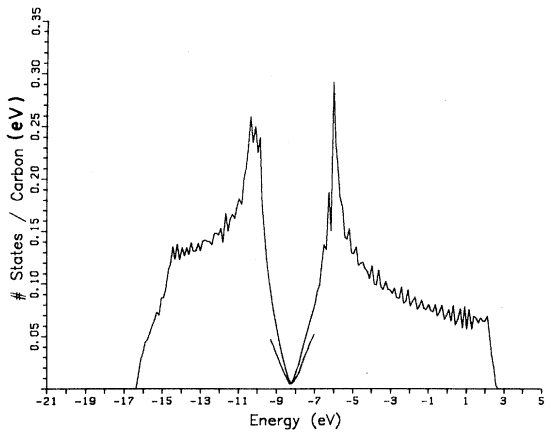

FIG. 8. Density of states obtained from JD model fit to first-principles bands (upper curve). Also shown for limited energy range is dos obtained from SWMc fit (lower curve).

C. Fermi surface and Fermi-surface properties

The Fermi surface corresponding to the energy $E_F = -0.025$ eV is shown in Fig. 9. For comparison, we performed the same procedure for the JD model and obtained a slightly different surface also shown in Fig. 9. In addition to what is shown in the figure, the SWMc and JD models include three additional legs that provide a thicker overall cross section between the electron-hole junction. These details are omitted from the figure since they are not resolvable to the precision with which the figure is drawn. Also hidden from view are the hole pockets near the *H* point.

Several measurable quantities that depend on the Fermi surface were computed numerically and are summarized in Table III. The de Haas–van Alphen frequencies are related to extremal cross sections of the Fermi surface (A_{ex}) and were comput-

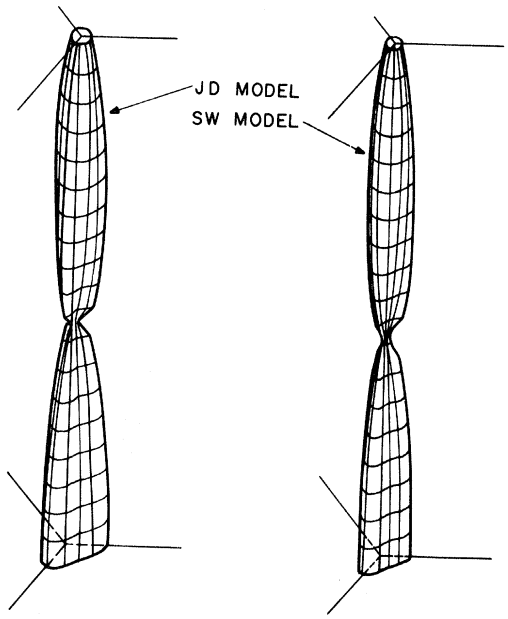

FIG. 9. Fermi surfaces of graphite from two different parametrized fits of bands. *H* (*K*) point is at intersection of upper (lower) three axes [see Fig. 10(h).]

TABLE III. Graphite Fermi-surface characteristics, de Haas–van Alphen periods (10^{-5} G^{-1}) and cyclotron masses.

	Majority electrons (K)	Majority holes	Minority holes (H)	
$F(H)$				
calculated	1.68	2.37	13.7	
Experiment				
Refs. 23 and 73	1.61	2.20	13.5	
$M(H)$				
calculated	$0.045m_0$	$0.033m_0$	$0.006m_0$	
Experiment	$0.06m_0$	$0.04m_0$	$0.002m_0$	
	Plasma frequencies (eV)			
	Present	Typical[a] SWMc params.	Nakao[b]	McClure[c]
$\hbar\omega_a$	0.46	0.44	0.83	0.17
$\hbar\omega_c$	0.04	0.04	0.07	0.01

[a]See Table I, first column.
[b]From Ref. 64.
[c]From Ref. 63.

ed for field parallel to the k_z axis, as follows:

$$F(\hat{H})=\frac{c\hbar}{2\pi e}A_{\rm ex}(\hat{H}) .$$

The cyclotron effective masses were computed from the relation

$$m^*=m_c\frac{\hbar^2}{2\pi}\int_0^{2\pi}\frac{K_\perp d\phi}{|\hat{K}_\perp\cdot\vec{\nabla}_K E|} ,$$

and are experimentally determined by magnetoreflection experiments[24] that give the Landau-level separations. $\vec{K}_\perp$ is the wave vector perpendicular to the layer planes. The agreement with experiment is good.

In some materials low-frequency optical properties can be described by the dielectric tensor:

$$\epsilon^{ij}=\delta_{ij}+\epsilon^{ij}_{\rm inter}+\epsilon^{ij}_{\rm intra} .$$

$\epsilon^{ij}_{\rm intra}$ has the form

$$\epsilon^{ij}_{\rm intra}=\sum_\alpha\frac{[(\omega_p^\alpha)^{ij}]^2}{\omega(\omega+i/\tau^\alpha)} ,$$

where the sum is over different carriers. τ^α and ω_p^α are scattering time and the plasma frequency, respectively, associated with carrier α. The plasma frequency is given by the Fermi-surface integral:

$$[(\omega_p^\alpha)^{ij}]^2=\frac{4\pi e^2}{\hbar^2}\frac{2}{(2\pi)^3}\int_{\rm FS}\frac{d\vec{s}}{|\nabla_K E|}\left[\frac{\partial E}{\partial K_i}\frac{\partial E}{\partial K_j}\right] .$$

For graphite there are only two independent components of ω^{ij} associated with the π-band carriers, in-plane and c-axis frequencies ω_a,ω_c.

$$\omega_a^2=\frac{(\omega^{xx})^2+(\omega^{yy})^2}{2} ,$$

$$\omega_c^2=(\omega^{zz})^2 .$$

Table III shows the values of plasma frequency obtained from our calculations as well as those based on a generally accepted set of SWMc parameters. We have also included plasma frequencies obtained by McClure[63] from estimates of electron density and effective mass as well as those calculated by Nakao.[64] Our values fall between the results of McClure and Nakao. For graphite, experimental determination of plasma frequencies is very difficult if not impossible because of the screening due to interband transition.

D. Constant-energy surfaces

Several constant-energy surfaces above and below the Fermi level were computed from the JD fit. These are shown in Fig. 10. While graphite rigid-band analyses are generally applicable only in the dilute limit, these surfaces would correspond to Fermi surfaces of low-stage graphite-intercalation compounds if the only effect of intercalation was to introduce additional carriers and if structural changes leading to zone folding could be neglected.

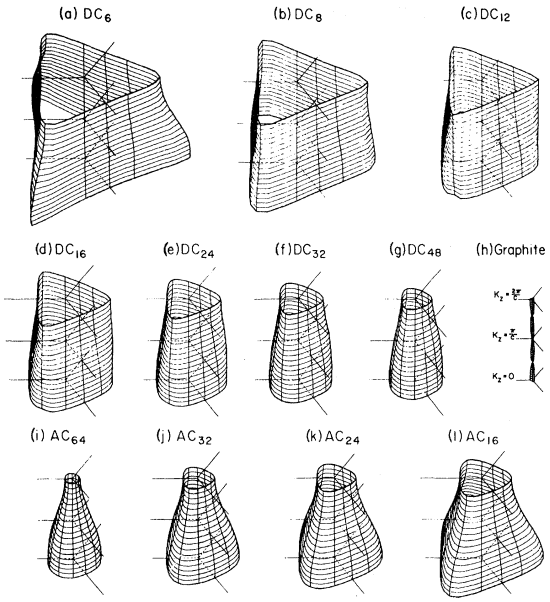

FIG. 10. Constant-energy surfaces of graphite for selected energy levels (see text, Table IV).

For this reason the figures are labeled by the stoichiometries of compounds with 100% charge transfer and the corresponding energy level is derived from the graphite density of states. For example, DC_8 has $\frac{1}{8}$ extra electron per carbon and AC_{24} has $\frac{1}{24}$ extra hole per carbon. Further, AC_{24} could correspond to a stage-two acceptor with 50% charge transfer or a stage-one acceptor with 25% charge transfer. The energy levels corresponding to the figures are given in Table IV along with additional "Fermi"-surface data that in some instances could be used as a guide to bracket the range of values for actual compounds. The double-sheeted surfaces are shown in an extended-zone scheme for clarity.

The constant-energy surfaces show more clearly than the band structure the asymmetry of the bands above and below the Fermi level of graphite. The (d) and (l) figures are approximately the same distance above and below the Fermi level, respectively. The dimples in surface (c) and (d) are caused by the crossover of the upper π bands, which can be seen between M and K. The sharpness of the corners in the larger figures is due to the limited resolution.

V. DISCUSSION

We will now compare our band-structure calculation with other theoretical studies and experimental investigations by focusing on certain key band separations as listed in Table V. The three-dimensional LCAO calculation of Willis *et al.*,[18] is closest to ours for the levels up to and including

TABLE IV. Constant-energy surface properties.

Label (see Fig. 10)		Extra charge per carbon	$E_{const.}$ (eV)	DOS (states per carbon per eV) $N(E_F)$	Lower band ($k_z=0$) dHvA (G)	Lower band ($k_z=0$) Cyclotron mass (m_e)	Upper band ($k_z=0$) dHvA (G)	Upper band ($k_z=0$) Cyclotron mass (m_e)
(a)	DC_6	−0.166 67	−6.010	0.23	4.9×10^7	0.74	7.5×10^7	1.5
(b)	DC_8	−0.125	−6.264	0.19	3.9×10^7	0.62	5.9×10^7	1.05
(c)	DC_{12}	−0.083 33	−6.532	0.11	1.5×10^7	0.49	4.0×10^7	0.67
(d)	DC_{16}	−0.0625	−6.709	0.10	1.8×10^7	0.44	3.1×10^7	0.51
(e)	DC_{24}	−0.041 67	−6.936	0.080	1.1×10^7	0.33	2.2×10^7	0.40
(f)	DC_{32}	−0.031 25	−7.074	0.070	7.0×10^6	0.27	1.7×10^7	0.35
(g)	DC_{48}	−0.020 83	−7.220	0.061	3.5×10^6	0.21	1.3×10^7	0.29
(h)	Graphite	0.0	−8.06	1.2×10^{-4}[a]	5.9×10^4	0.045		
(i)	AC_{64}	+ 0.015 03	−8.702	0.036	8.8×10^5	−0.093[b]	1.3×10^7	−0.37
(not shown)	AC_{48}	+ 0.020 83	−8.758	0.044	1.7×10^6	−0.12	1.6×10^7	−0.43
(j)	AC_{32}	+ 0.031 25	−8.986	0.055	3.8×10^6	−0.16	2.3×10^7	−0.53
(k)	AC_{24}	+ 0.041 67	−9.117	0.073	5.9×10^6	−0.20	2.9×10^7	−0.63
(l)	AC_{16}	+ 0.0625	−9.345	0.098	1.0×10^7	−0.27	4.2×10^7	−0.84

[a]Calculated from the four-parameter model $N(E_f)=(2/\pi^5\sqrt{3})\gamma_1/\gamma_0^2$.
[b]Negative mass indicates hole carriers.

TABLE V. Comparison of band-structure calculations and measurements[a] (eV).

	HRG (KKR) Present results	Cellular sph. sym. Mallet (Ref. 21)	ext. LCAO Batra (Ref. 17)	LCAO Willis *et al.* (Ref. 18)	Sph. symm. Pseudopot. HJ (Ref. 19)	Ext. Hückel Zunger (Ref. 12)	LCAO PE (Ref. 7)	Experiment (Ref.)
$\Gamma_1^+-\Gamma_5^+$								
σBW	14.8(16)	17	20.7	16	NA[b]	16.5	14.3	
$\Gamma_5^+-\Gamma_1^+$								
occ-unocc	11.76(2.44)	5.4	12.5	12	9	12.5	12.2	11.5±1 (18)
$\Gamma_3^+-\Gamma_3^+$								
πBW	18.63(28)	19	15	19	NA	17.5	17.7	
$\Gamma_3^+-\Gamma_2^-$								
πsep	1.65(3.8)	2.0	1.3	1.8	NA			0.9±0.3 (35)
$\Gamma_3^+-\Gamma_1^+$	11.3(8.0)	10	16	12.5	NA	16	11.6	11 ±0.3 (35)
$E_f-\Gamma_1^+$								
Val. BW	19.5(17.5)	18.6	21.7	20.7	NA	20	19.3	20.6±0.3 (35)
$M_3^+-M_4^-$	4.3(4.4)	4.1	4.5	4.3	4.0	4.8	4.6	4.6 (44)
$M_4^--M_3^+$								
K_4-K_2	1.04(3.2)	1.4	0.8	1.3	1.8			1.6 (33)

[a]For optical selection rules see Ref. 71.

[b]NA—not available.

the conduction σ bands. In fact their conduction bands and those of Nagayoshi *et al.*[10] are in the best qualitative agreement with the present work, specifically the crossing of the Σ_1,Σ_4 levels between Γ and M, a feature which is absent from all other studies.

There is also much agreement with the single-layer calculation of Painter and Ellis.[7] This can probably be accounted for by the similarity in the crystal potentials. In all these calculations the same approximation to the exchange potential was used with the same α parameter of 0.76. Samuelson *et al.*[17] used the same prescription but with $\alpha=0.667$ and, while their overall results are similar, the Fermi-level bands have too little dispersion to obtain reasonable estimates of the SWMc parameters. Mallett[21] used a spherically symmetric potential with the cellular method and Haeringen and Junginger[19] used a spherically symmetric pseudopotential. Even though the use of a spherically symmetric potential is not appropriate for graphite these calculations were *ab initio* and could provide a starting point for a more accurate calculation. This conjecture is strengthened by the fact that they are similar in some ways to our muffin-tin band structure. In particular a Γ_1^+ level in Mallett's calculation, just above the σ valence bands, differs by 0.1 eV from a corresponding level in our muffin-tin band structure. This level is strongly affected by the potential away from the atomic cores and moves upward by 9.5 eV when the exact interstitial potential is included.

The SWMc parameters estimated from our band structure are in very good agreement with those obtained experimentally. This is shown in Table VI where parameter values from other calculations are also included. Although the values for γ_3 and γ_5 are slightly smaller than those suggested by experiments, we feel the agreement is remarkable given that the calculation was completely *ab initio*. The results of Nagayoshi *et al.*[11] are also very good, although their potential had an adjustable parameter that was chosen to fit optical data.

Recently, magnetoreflection experiments[65] suggest a negative sign for Δ, in disagreement with our results. Furthermore, our K_4-K_2 separation is somewhat smaller than that suggested by optical studies leading to a smaller value of γ_0. These and other discrepancies might be improved somewhat if the KKR basis was extended to much higher energies. Self-consistency might also improve the agreement with experimental results although we do not expect self-consistency to be as crucial here as for the intercalation compounds. The complexity of our *ab initio* appproach renders the inclusion of self-consistency computationally intractable at the present time. Nevertheless, this calculation is successful, on the one hand, by virtue of the good

TABLE VI. Comparison: experiment and theory SWMc parameters (eV).

	Experiments	Present results	Mallet (Ref. 21)	Batra (Ref. 17)	HJ (Ref. 19)	S. C. LCAO Zunger (Ref. 12)	PE (Ref. 7)	Nagayoshi *et al.* (Ref. 11)
γ_0	3.16	2.92				2.53		2.73
γ_1	0.39	0.27	0.36	0.2	0.41	0.32	0.25	0.32
γ_2	−0.19	−0.022	−0.045	−0.003	−0.043		0.022	
γ_3	0.28	0.15						0.29
γ_4	0.044	0.10						0.15
γ_5	0.038	0.0063	0.0004		0.033		0.003	0.021
Δ	−0.008	0.0079	−0.0009	−0.004	0.42		0.09	−0.017
E_F	−0.024	−0.025						−0.021

agreement with experiments that measure moderately large level separations and, on the other hand, by supplying reasonable SWMc parameters and a Fermi surface that is in quantitative agreement with experimental results.

We conclude that this method should work well for other highly anisotropic materials such as the intercalation compounds of graphite, although extension to self-consistency may be necessary in such cases. Nevertheless, a carefully conceived model for the potential should give reasonable results.

ACKNOWLEDGMENTS

We would like to thank David DiVincenzo and Natalie Holzwarth for their assistance and discussion during the course of this work. We would also like to thank John Fischer and other members of the graphite group for their encouragement and support. Finally, without the patience and good nature of the staff of the Moore School Computing Facility, this work would not have been possible. This work was supported by the National Science Foundation, Materials Research Laboratory program under Grant No. DMR-7923647 and also by ARO Contract No. DAAG-29-80-k-0019.

APPENDIX A: SWMc MODEL

The SWMc Hamiltonian has the form:

$$H=\begin{bmatrix} \epsilon_1^0 & 0 & H_{13} & H_{13}^* \\ 0 & \epsilon_2^0 & H_{23} & -H_{23}^* \\ H_{13}^* & H_{23}^* & \epsilon_3^0 & H_{33} \\ H_{13} & -H_{23} & H_{33}^* & \epsilon_3^0 \end{bmatrix},$$

where

$$\epsilon_1^0=\Delta+2\gamma_1\cos\beta+2\gamma_5\cos^2\beta\,,$$

$$\epsilon_2^0=\Delta-2\gamma_1\cos\beta+2\gamma_5\cos^2\beta\,,$$

$$\epsilon_3^0=2\gamma_2\cos^2\beta\,,$$

$$H_{13}=\frac{\sqrt{3}}{2\sqrt{2}}(2\gamma_4\cos\beta-\gamma_0)a\kappa e^{i\alpha}\,,$$

$$H_{23}=\frac{\sqrt{3}}{2\sqrt{2}}(2\gamma_4\cos\beta+\gamma_0)a\kappa e^{i\alpha}\,,$$

$$H_{33}=\sqrt{3}(\gamma_3\cos\beta)a\kappa e^{i\alpha}\,,$$

$\beta=k_zc/2$, α is polar angle about zone edge ($\alpha=0°$ toward Γ). $\kappa=(k_x^2+k_y^2)^{1/2}$ (origin at K point) and a,c are graphite lattice constants.

This Hamiltonian is based on a perturbation expansion and is valid only for small κ. A good discussion of this and related models can be found in the review article by Spain.[31]

APPENDIX B: JD MODEL

The full-zone π-band expansion for graphite was first introduced by Johnson and Dresselhaus.[16] Since then many variants of this model have been developed and applied to similar systems. Our reference to the JD model stands for the entire class of such expansions. Blinowski *et al.*[66] and Holzwarth[62] used versions of this model appropriate for optical and transport properties of graphite-intercalation compounds (GIC's). Saffran and DiSalvo[67] used essentially a very primitive version of this model to compute magnetic susceptibilities of GIC's.

The particular form used in this work is as follows:

$$H=\begin{bmatrix} H_{AA} & H_{AA'} & H_{AB} & H_{AB'} \\ H^*_{AA'} & H_{AA} & H^*_{AB'} & H^*_{AB} \\ H^*_{AB} & H_{AB'} & H_{BB} & H_{BB'} \\ H^*_{AB'} & H_{AB} & H^*_{BB'} & H_{BB} \end{bmatrix},$$

$$H_{AA}=a^{000}_{AA}(3)+a^{100}_{AA}[\cos(\xi_x)+2\cos(\tfrac{1}{2}\xi_x)\cos(\tfrac{1}{2}\xi_y)]+a^{002}_{AA}[3\cos(2\xi_z)],$$

$$H_{BB}=a^{000}_{BB}(3)+a^{100}_{BB}[\cos(\xi_x)+2\cos(\tfrac{1}{2}\xi_x)\cos(\tfrac{1}{2}\xi_y)]+a^{002}_{BB}[3\cos(2\xi_z)],$$

$$H_{AB}=a^{0\bar{1}0}_{AB}[e^{-i(1/3)\xi_y}+2\cos(\tfrac{1}{2}\xi_x)e^{i(1/3)\xi_y}]+a^{020}_{AB}[e^{i(2/3)\xi_y}+2\cos(\xi_x)e^{-i(1/3)\xi_y}]$$
$$+a^{120}_{AB}[\cos(\xi_x)e^{i(2/3)\xi_y}+\cos(\tfrac{3}{2}\xi_x)e^{i(1/6)\xi_y}+\cos(\tfrac{1}{2}\xi_x)e^{-i(5/6)\xi_y}],$$

$$H_{AB'}=a^{0\bar{1}1}_{AB'}[e^{i(1/3)\xi_y}+2\cos(\tfrac{1}{2}\xi_x)e^{-i(1/6)\xi_y}]\cos\xi_z,$$

$$H_{BB'}=a^{0\bar{1}1}_{BB'}[e^{-i(1/3)\xi_y}+2\cos(\tfrac{1}{2}\xi_x)e^{i(1/6)\xi_y}]\cos\xi_z,$$

$$H_{AA'}=a^{001}_{AA'}(3\cos\xi_z),$$

where $\xi_x=ak_x$, $\xi_y=a\sqrt{3}k_y$, $\xi_z=\frac{1}{2}ck_z$, and following the definition in the original article, the notation $a^{ijk}_{\alpha\beta}$ denotes the matrix element between sites α and β in unit cells located relative to each other by $T=i\hat{t}_x+j\hat{t}_y+k\hat{t}_z$. The overbar indicates a negative number. A different coordinate system was used here, accounting for the different notation of some of the parameters.

APPENDIX C: SOME CALCULATION DETAILS

This appendix provides a brief description of some of the specific computational aspects concerning the present work. A more general discussion is found in Sec. III and in Ref. 48.

In the first step of the KKR procedure symmetry is used to simplify the evaluation of the matrix elements

$$V_{lm,l'm'}(r)=\int Y^*_{lm}(\hat{r})V(\vec{r})Y_{l'm'}(\hat{r})\,d^2r, \quad |\vec{r}|=\text{const}$$

which appear in the system:

$$\sum_{l'm'}\left\{\left[\frac{-\hbar^2}{2m}\left[\frac{d^2}{dr^2}-\frac{l'(l'+1)}{r^2}\right]-E\right]\delta_{lm,l'm'}+V_{lml'm'}(r)\right\}P^i_{El'm'}(r)=0,$$

where

$$P^i_{Elm}(r)=rR^i_{Elm}(r)$$

and

$$\phi^i_E(\vec{r})=\sum_{lm}R^i_{Elm}(r)Y_{lm}(\hat{r})$$

are the solutions to Schrödinger's equation within a muffin-tin sphere. From symmetry we determine which matrix elements are nonzero, then by expanding products of spherical harmonics into crystal harmonics it is possible to further reduce the total number of integrations and stored integrals.

TABLE VII. Relationship between SWMc parameters and JD parameters.

$\gamma_0=-a^{0\bar{1}0}_{AB}+2a^{020}_{AB}+\frac{1}{2}a^{120}_{AB}$
$\gamma_1=\frac{3}{2}a^{001}_{AA'}$
$\gamma_2=3a^{002}_{BB}$
$\gamma_3=\frac{1}{2}a^{0\bar{1}1}_{BB'}$
$\gamma_4=\frac{1}{2}a^{0\bar{1}1}_{AB'}$
$\gamma_5=3a^{002}_{AA}$
$\Delta=3[a^{000}_{AA}-a^{000}_{BB}-\frac{1}{2}(a^{100}_{AA}-a^{100}_{BB})+a^{002}_{BB}-a^{002}_{AA}]$

For graphite $l=2$ expansion, there are 12 nonzero $V_{lml'm'}(r)$ components and these can be expressed in terms of four crystal harmonics, a substantial reduction from the original 45 integrals:

$$V_{lml'm'}(r)=\sum_{\alpha} I^{\alpha}_{lml'm'} \int Z_{\alpha}(\hat{r})V(\vec{r})\,d^2r \ ,$$

$$|\vec{r}\,|=\text{const}$$

where the I coefficients are constant and, where

$$Z_1(\hat{r})=1 \ ,$$

$$Z_2(\hat{r})=(\tfrac{5}{4})^{1/2}(3z^2-1) \ ,$$

$$Z_3(\hat{r})=(\tfrac{35}{8})^{1/2}(3y^2-x^2)x \ ,$$

$$Z_4(\hat{r})=(\tfrac{105}{8})^{1/2}[z^4-\tfrac{6}{7}(\tfrac{5}{4})^{1/2}(3z^2-1)-\tfrac{1}{5}] \ ,$$

are from Ref. 68. These crystal harmonics are orthogonal and invariant under the operations of the group D_{3h}. Because of the symmetry we need only perform the angular integrations over a fraction of the unit sphere which for graphite is $\frac{1}{12}$. For convenience we chose a $\frac{1}{4}$ spherical domain.[69]

The Δ_{NM} [see Eq. (2), Ref. 48] matrix elements were computed in an irreducible section of the interstitial region shown in Fig. 11. The integration algorithm was the 3D Gaussian technique described in Ref. 48. The coordinate system was chosen to most conveniently accommodate this step of the calculation.

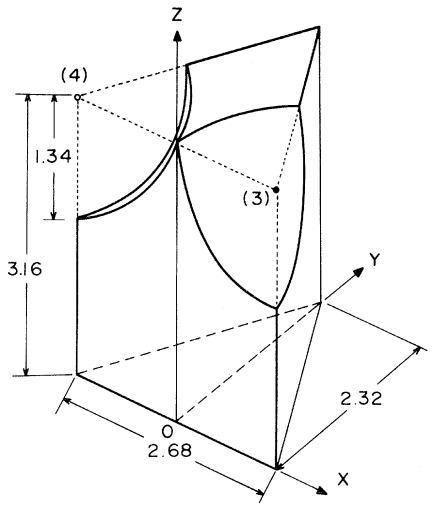

FIG. 11. Interstitial region of irreducible sector. Dimensions are in atomic units.

[1]P. R. Wallace, Phys. Rev. 71, 622 (1947).
[2]C. A. Coulson and R. Taylor, Proc. R. Soc. London Ser. A 65, 815 (1952).
[3]W. M. Lomer, Proc. R. Soc. London Ser. A 277, 330 (1955).
[4]D. F Johnson, Proc. R. Soc. London Ser. A 227, 349 (1955); 237, 48 (1956).
[5]J. C. Slonczewski and P. R. Weiss, Phys. Rev. 109, 272 (1958).
[6]F. Bassani and G. Pastori Parravicini, Nuovo Cimento B 50, 95 (1967).
[7]G. S. Painter and D. E. Ellis, Phys. Rev. B 1, 4747 (1970).
[8]M. Tsukada, K. Nakao, Y. Uemura, and Nagai, J. Phys. Soc. Jpn. 32, 54 (1972).
[9]H. Nagayoshi, M. Tsukada, K. Nakao, and Y. Uemura, J. Phys. Soc. Jpn. 35, 396 (1973).
[10]H. Nagayoshi, K. Nakao, and Y. Uemura, J. Phys. Soc. Jpn. 41, 1480 (1976).
[11]H. Nagayoshi, K. Nakao, and Y. Uemura, Solid State Commun. 10, 225 (1976).
[12]A. Zunger, Phys. Rev. B 17, 626 (1978).
[13]R. Dovesi, C. Pisani, and C. Roetti, Int. J. Quantum Chem. 17, 517 (1980).
[14]P. G. Perkins, A. K. Marwaha, and J. P. Stewart, Theor. Chim. Acta 57 (1980); LCAO (CNDO), self-consistent.
[15]J. W. McClure, Phys. Rev. 108, 612 (1957).
[16]L. G. Johnson and G. Dresselhaus, Phys. Rev. B 7, 2275 (1973).
[17]L. Samuelson, I. P. Batra, and C. Roetti, Solid State Commun. 33, 817 (1980); I. P. Batra and L. Samuelson, Synth. Met. 1, 223 (1979/80).
[18]R. F. Willis, B. Fitton, and G. S. Painter, Phys. Rev. B 9, 1926 (1974).
[19]W. van Haeringen and H. G. Junginger, Solid State Commun. 7, 1723 (1969).
[20]N. A. W. Holzwarth, S. G. Louie, and S. Rabii (unpublished).
[21]C. Mallett, J. Phys. C (GB) 14, L213 (1981).
[22]J. W. McClure, Phys. Rev. 119, 606 (1960).
[23]D. E. Soule, IBM J. Res. Dev. 8, 268 (1964).
[24]S. J. Williamson, S. Foner, and M. S. Dresselhaus, Phys. Rev. 104A, 1429 (1965).
[25]J. A. Woolam, Phys. Rev. B 4, 3393 (1971).
[26]M. S. Dresselhaus and J. G. Mabroides, IBM J. Res. Dev. 8, 262 (1964); Carbon 1, 263 (1964); A. Misu, E. E. Mendez, and M. S. Dresselhaus, J. Phys. Soc. Jpn. 47, 199 (1979).
[27]P. Nozières, Phys. Rev. 109, 1510 (1958).
[28]T. Uda, H. Ushio, and Y. Uemura, J. Phys. Soc. Jpn. 36, 652 (1974).
[29]S. J. Williamson, M. Surma, H. C. Praddaude, R. A. Patten, and J. K. Furdyna, Solid State Commun. 4, 37 (1966).
[30]I. L. Spain, in *Chemistry and Physics of Carbon*, edited

by P. L. Walker and P. A. Thrower (Dekker, New York, 1973), Vol. 8.
[31]I. L. Spain, in *Chemistry and Physics of Carbon,* edited by P. L. Walker, Jr. and P. A. Thrower (Dekker, New York, 1980), Vol. 8.
[32]J. W. McClure, in *Physics of Semimetals and Narrow Bandgap Semiconductors,* edited by D. L. Carter and R. T. Bate (Pergamon, New York, 1971).
[33]R. F. Willis, B. Deuerbacher, and B. Fitton, Phys. Rev. B 4, 2441 (1971).
[34]A. Bianconi, S. B. M. Hagstom, and R. Z. Bachrach, Phys. Rev. B 16, 5543 (1977).
[35]I. T. McGovern, W. Eberhardt, E. W. Plummer, and J. E. Fischer, Physica 99B, 415 (1980).
[36]R. F. Willis and B. Fitton, J. Vac. Sci. Technol. 9, 651 (1972).
[37]J. M. Thomas, E. L. Evans, M. Barber, and P. Swift, Trans. Faraday Soc. 67, 1875 (1971).
[38]J. M. Muller, F. Feser, G. Wiech, and A. Faessler, Phys. Lett. 44A, 263 (1973).
[39]F. R. McFreely, S. P. Kowalczyk, L. Ley, R. G. Cavell, R. R. Pollak, and D. A. Shirley, Phys. Rev. B 9, 5268 (1974).
[40]F. C. Chalkin, Proc. R. Soc. London Ser. A 194, 42 (1948).
[41]E. Tosatti and F. Bassani, Nuovo Cimento 65, 161 (1970).
[42]E. A. Taft and H. R. Philipp, Phys. Rev. 138A, 197 (1965).
[43]S. Ergun, J. B. Yasinsky, and J. R. Townsend, Carbon 5, 403 (1967).
[44]D. L. Greenaway, G. Harbeke, F. Bassani, and E. Tosatti, Phys. Rev. 178, 1340 (1969).
[45]G. Guizetti, L. Nosenzo, E. Reguzzoni, and G. Samoggia, Phys. Rev. Lett. 31, 154 (1973).
[46]W. S. Boyle and P. Nozières, Phys. Rev. 111, 782 (1958).
[47]N. A. W. Holzwarth, S. Rabii, and L. A. Girifalco, Phys. Rev. B 18, 5190 (1978).
[48]D. P. DiVincenzo and S. Rabii, preceding paper, Phys. Rev. B 25, 4110 (1982)
[49]J. D. Bernal, Proc. R. Soc. London Ser. A 106, 749 (1924).
[50]D. Sands, *Introduction to Crystallography* (Benjamin-Cummings, Reading, Mass., 1969).
[51]*International Tables of X-Ray Crystallography,* edited by G. Wycoff (Kynoch, London, 1952).
[52]J. F. Cornwell, *Group Theory and Energy Bands in Solids* (North-Holland, Amsterdam, 1969).
[53]F. Herman and S. Skillman, *Atomic Structure Calculations* (Prentice-Hall, Englewood Cliffs, 1963).
[54]J. C. Slater, *The Self-Consistent Field for Molecules and Solids* (Mc-Graw-Hill, New York, 1974).
[55]K. Schwartz, Phys. Rev. B 5, 2466 (1972).
[56]G. S. Painter, Phys. Rev. B 7, 3520 (1973).
[57]J. Korringa, Physica (Utrecht) 13, 392 91947).
[58]W. Kohn and N. Rostoker, Phys. Rev. 94, 1111 (1954).
[59]J. C. Slater, *Symmetry and Energy Bands In Crystals* (Dover, New York, 1972).
[60]There are various techniques to approximate certain of these integrals. See, for example, D. H. Chadi and M. L. Cohen, Phys. Rev. B 8, 5747 (1973); A. B. Chen, *ibid.* 16, 3291 (1977).
[61]P. R. Bevington, *Data Reduction and Error Analysis for the Physical Sciences* (McGraw-Hill, New York, 1969).
[62]N. A. W. Holzwarth, Phys. Rev. B 21, 3655 (1980).
[63]J. W. McClure, IBM J. Res. Dev. 8, 255 (1964).
[64]K. Nakao, J. Phys. Soc. Jpn. 47, 208 (1979).
[65]W. W. Toy, M. S. Dresselhaus, and G. Dresselhaus, Phys. Rev. B 15, 4077 (1977).
[66]J. Blinowski, N. H. Hau, C. Ragaux, J. P. Vieren, G. Furdin, and J. Melin, J. Phys. (Paris) 41, 47 (1980).
[67]S. A. Saffran and F. J. DiSalvo, Phys. Rev. B 20, 4889 (1979).
[68]D. G. Bell, Rev. Mod. Phys. 26, 311 (1954), reprinted in *Symmetry in the Solid State,* edited by R. S. Knox and A. Gold (Benjamin, New York, 1964), p. 299.
[69]A. M. Stroud, *Approximate Calculation of Multiple Integrals* (Prentice-Hall, Englewood Cliffs, 1971).
[70]E. Mendez, A. Misu, and M. S. Dresselhaus, Phys. Rev. B 21 827 (1980).
[71]R. L. Benbow, Phys. Rev. B 22, 3775 (1980).